A&A 379, 436–452 (2001)
DOI: 10.1051/0004-6361:20011325

Astronomy & Astrophysics

ESO imaging survey

Pre-FLAMES survey: Observations of selected stellar fields⋆

Y. Momany[1,2], B. Vandame[1], S. Zaggia[1,3], R. P. Mignani[1], L. da Costa[1], S. Arnouts[1], M. A. T. Groenewegen[1], E. Hatziminaoglou[1], R. Madejsky[1,5], C. Rité[1,6], M. Schirmer[4], and R. Slijkhuis[1]

[1] European Southern Observatory, Karl-Schwarzschild-Str. 2, 85748 Garching b. München, Germany
[2] Dipartimento di Astronomia, Universitá di Padova, Vicolo dell'Osservatorio 5, 35122 Padova, Italy
[3] Osservatorio Astronomico di Trieste, Via G. B. Tiepolo 11, 34131 Trieste, Italy
[4] Max-Planck Institut für Astrophysik, Karl-Schwarzschild-Str. 1, 85748 Garching b. München, Germany
[5] Universidade Estadual de Feira de Santana, Campus Universitário, Feira de Santana, BA, Brazil
[6] Observatório Nacional, Rua Gen. José Cristino 77, Rio de Janerio, R.J., Brasil

Received 30 July 2001 / Accepted 18 September 2001

Abstract. This paper presents the first set of fully calibrated images and associated stellar catalogs of the Pre-FLAMES survey being carried out by the ESO Imaging Survey (EIS) project. The primary goal of this survey is to provide the ESO community with data sets from which suitable target lists can be extracted for follow-up observations with the new VLT facility FLAMES (Fiber Large Array Multi Element Spectrograph). For this purpose, 160 stellar fields have been selected for observations in B, V and I using the 8k × 8k Wide Field Imager (WFI) at the MPG/ESO 2.2 m telescope at La Silla. Out of those, over 100 fields have already been observed. The list of selected fields includes open clusters, globular clusters, regions in the Galaxy bulge, dwarf spheroidal galaxies in the vicinity of the Milky Way, contiguous regions of SMC and LMC and few nearby clusters of galaxies. The present paper discusses the results obtained for a small subset of these data, which include four open clusters (M 67, NGC 2477, NGC 2506 and Berkeley 20) and two regions of the SMC. These data have been used to assess the observing strategy adopted, a combination of short- and long-exposures, and to define suitable reduction techniques and procedures for the preparation of input catalogs for FLAMES. In order to minimize light losses due to misplacements of FLAMES fibers, the astrometric calibration of crowded stellar fields is a critical issue. The impact of different swarping techniques and different reference catalogs on the astrometric calibration of the images is evaluated and compared to those of other authors. From this comparison, one finds that both USNO 2.0 and the recently released GSC 2.2 yield comparable results with the positional differences having a rms of about 0.15 arcsec, well within the requirements (0.2 arcsec) specified by the FLAMES science team. The internal accuracy of the astrometry is estimated to be $\lesssim$0.1 arcsec, primarily limited by the reference catalog used. The major difference between these catalogs is the systematic variation of the positional residuals as a function of the apparent magnitude of the objects, with the GSC 2.2 yielding by far the best results. The astrometric calibration of the images presented here is based on the USNO 2.0 catalog because not all fields considered are covered by the current release of the GSC 2.2. Future EIS calibrations will be done using the GSC 2.2 catalog. The extraction and photometric measurements of stellar sources are carried out using a PSF fitting technique. Comparison with results available in the literature shows that the photometric measurements are in good agreement, apart from possible zero-point offsets, with the magnitude differences having a scatter of ∼0.06 mag at $V = 20$ mag. This demonstrates that the data allow for the selection of robust targets down to the expected spectroscopic limit of FLAMES. The combination of catalogs extracted from the short and long-exposures allows one to produce color-magnitude diagrams (CMD) spanning ∼13 mag in V and reaching a limiting magnitude of $V \sim 22-23$. These data have also been combined with data from the Two Micron All Sky Survey (2MASS) survey allowing for a better color-based object classification and target selection. The Pre-Flames (PF) survey data meet the requirements of FLAMES, and provide a good starting point for detailed studies of the examined systems. The images and catalogs presented here are publicly available and can be requested from the URL address "`http://www.eso.org/eis`".

Key words. techniques: image processing – astronomical data bases: miscellaneous

Send offprint requests to: Y. Momany,
e-mail: `ymomany@eso.org`

⋆ Based on observations collected at the European Southern Observatory, La Silla, Chile within program ESO 164.O-O561.

1. Introduction

The ESO Imaging Survey (EIS) project was conceived with the purpose of producing data sets matching the

foreseen scientific goals and requirements of different VLT instruments (e.g.Renzini & da Costa 1997). With this in mind, EIS has been carrying out for the past two years the Deep Public Survey (DPS), an optical/infrared deep survey of high-galactic latitude fields, and the so-called Pre-FLAMES (PF) survey. The latter survey consists of selected stellar fields well matched to VIMOS and FLAMES (Fibre Large Array Multi Element Spectrograph, Pasquini et al. 2000) capabilities, respectively.

FLAMES, which will be installed on the A Nasmyth platform of the VLT Kueyen telescope, consists of a fiber positioner, a dedicated fiber-fed spectrograph (GIRAFFE) and a fiber link to the UVES spectrograph located on the B Nasmyth platform. The fiber positioner covers a corrected field of view of $\simeq$25 arcmin in diameter. GIRAFFE will be fed by fibers in one of the following ways: (a) 130 fibers, 1.2 arcsec in diameter, in the MEDUSA configuration; (b) 15 deployable integral field units (IFUs, 2×3 square arcsec with 20 fibers each); (c) one central large unit (ARGUS, 11.5×7.3 square arcsec with 308 fibers). GIRAFFE will have two gratings with a resolving power of $R = 5000$–9000 and $R = 15\,000$–$25\,000$, depending on the fiber mode used. The corresponding spectral coverage will be $\sim$50–120 nm and $\sim$20–50 nm, respectively. The performance of the instrument can be illustrated by the following example: an exposure of one-hour with GIRAFFE in the MEDUSA mode of a $V = 20$ mag point source at $R = 15\,000$ is expected to yield a spectrum with a signal-to-noise ratio of 15 per resolution element. UVES will be fed by 8 fibers and will only use the red arm with a resolving power of $R \sim 45\,000$ and a spectral coverage of 200 nm. An important feature of the FLAMES setup is that it will allow for simultaneous observations with GIRAFFE and UVES.

The relatively small diameter of the fibers and the lack of an imaging mode require the preparation of target lists with accurate astrometry. The positional errors have to be small ($\lesssim$0.2 arcsec) in order to minimize the off-center losses. It is estimated that misplacing a fiber by $\sim$0.5 arcsec, during observations under seeing conditions typical of Paranal ($\sim$0.7 arcsec), would decrease the collected flux by $\simeq$50%. In addition, to take full advantage of GIRAFFE, multi-color source catalogs with reliable photometry (e.g.$\sim$0.03 mag at $V = 20$) over the large field-of-view of FLAMES are required for an adequate preselection of spectroscopic targets and their subsequent analysis.

Foreseeing the need to build suitable data sets for FLAMES, ESO's Working Group for public surveys recommended the EIS project to carry out an imaging survey of selected dense stellar fields, the so-called Pre-FLAMES (PF) Survey. The survey is being conducted with the Wide-Field Imager (WFI) at the MPG/ESO 2.2 m telescope, with a field of view (34×33 arcmin) comparable to that of FLAMES ($\simeq$25 arcmin in diameter). As in the case of other public surveys carried out by EIS, the ultimate goal has been not only to gather imaging data, but develop and test procedures to produce science grade products in the form of fully calibrated images and multi-color stellar catalogs, from which samples for observations with FLAMES can be extracted. The survey was designed to observe a suitable number of fields required for commissioning and first year of operation of FLAMES. The fields should have surface densities >1000 objects per square degree at the magnitude limit of FLAMES. Such fields will provide enough targets for the 130 fibers available in the MEDUSA mode. Considering that in a typical night the MEDUSA mode can produce around 1000 stellar spectra in five to ten different fields (Pasquini et al. 2000), this implies that approximately 500 stellar fields per year can be observed with FLAMES. To this end, a total of 160 fields were selected for observations from suggestions of users as compiled by the FLAMES team. Test runs were conducted during the first semester of 1999, as part of the EIS Pilot Survey. These earlier data helped to define the observing strategy of the PF survey which started in October 1999.

This paper presents the first set of data produced, which is used to assess the procedures being adopted in carrying out the observations and data reduction, to evaluate the results and to illustrate the scientific potential of the data once combined with the spectroscopic observations using FLAMES. This paper is organized as follows: Sect. 2 describes the observations conducted in the period November 27−29, 2000, one of 10 PF runs conducted so far. Section 3 describes the data reduction steps, while Sect. 4 presents a detailed discussion of the astrometric calibration, including the results of tests conducted using different swarping techniques and reference catalogs. In this paper, only the B and V images are presented, leaving to a subsequent paper the description of the reduction of the I band, which requires special treatment because of the strong and variable effects of fringing. The methods used in the preparation of the final photometric catalog, which includes source extraction in crowded fields, magnitude measurements based on PSF fitting, merging of catalogs extracted from short- and long-exposures and from different passbands, are discussed in Sect. 5. Section 6 describes the science products being released, which can be requested from the URL "`http://www.eso.org/eis`". A preliminary evaluation of the data is presented in Sect. 7 which presents and discusses the color-magnitude diagrams for the different stellar systems. Finally, in Sect. 8 the main results of the present paper are summarized and the future implementations are outlined.

2. Observations

The observations for the PF Survey are carried out using the WFI camera at the Cassegrain focus of the MPG/ES0 2.2 m telescope at the La Silla observatory. WFI is a focal reducer-type mosaic camera with 4×2 CCD chips of 2048×4098 pixels. Each chip covers a field of view of 8.12×16.25 arcmin with a projected pixel size of 0.238 arcsec. The 8 CCDs are physically separated by gaps of width 23.8 and 14.3 arcsec along the right

Table 1. Log of the November 27–29, 2000 observing run.

Target EIS name	RA (h m s)	Dec (d m s)	Night	Filter	Exp. Time (sec)	seeing (arcsec)
OC3 (Berkeley 20)	05 32 57.9	+00 13 04	27 Nov.	B	$2\times240+1\times30$	1.09−0.99
				V	$2\times240+1\times30$	1.02–1.14
SMC 5 (SMC)	00 56 45.0	−72 19 00	28 Nov.	B	$2\times240+1\times30$	1.36–1.29
				V	$2\times240+1\times30$	1.33–1.17
OC14 (NGC 2506)	08 00 10.7	−10 47 17	28 Nov.	B	$2\times240+1\times30$	0.90–0.79
				V	$2\times240+1\times30$	0.95–1.02
SMC 6 (SMC)	01 03 35.0	−72 19 00	29 Nov.	B	$2\times240+1\times30$	1.29–1.22
				V	$1\times240+1\times30$	1.29–1.33
OC12 (NGC 2477)	07 52 16.7	−38 32 48	29 Nov.	B	$2\times240+1\times30$	1.23–1.09
				V	$2\times240+1\times30$	1.09–1.07
OC99 (M 67)	08 51 22.0	+11 49 00	29 Nov.	B	$2\times240+1\times30$	1.36–1.21
				V	$2\times240+1\times30$	1.02–0.98

ascension and declination directions, respectively. The full field of view of the camera is thus 34× 33 arcmin, with a filling factor of 95.9%. More details about the instrument can be found on the La Silla web page (`http://www.ls.eso.org/lasilla`).

The adopted observing strategy for the PF survey was a compromise between number of required passbands, number of fields, exposure-time, filling factor, and observing overheads. The observations of PF fields were conducted in B, V and I to provide color information for the selection of objects. The integration time was split into a short-exposure of 30 s (SHALLOW), to avoid saturating bright objects, and two deeper exposures of four minutes each (DEEP). These were dithered by 30 arcsec both in right ascension and declination. The long exposures were sufficiently deep to reach the required signal-to-noise at the spectroscopic limit of FLAMES, while the short exposures allows one to recover saturated bright stars in the long exposures exposures (a gain of ∼4 mag). Bright stars are also necessary as guide stars for each FLAMES field, which should be in the same astrometric system as that of the target list.

Table 1 shows the log of the observations conducted in the period November 27–29, 2000. The table gives: in Col. (1) the EIS target identification and the name of the primary object being observed; in Cols. (2) and (3) the J2000 right ascension and declination; in Col. (4) the date of observation; in Col. (5) the filters used; in Col. (6) the exposure time and number of exposures for the SHALLOW and DEEP exposures; and in Col. (7) the seeing during the SHALLOW and DEEP exposures, respectively. As mentioned above, the I band images are not presented in this paper.

3. Data reduction

The WFI images were processed using the EIS pipeline, described in more detail by Arnouts et al. (2001) and Vandame et al. (2001). The basic reductions steps performed by the pipeline include the removal of the instrument signature (trimming, de-biasing and flat-field correction), pixel registration, removal of cosmic rays and other image artifacts, image swarping to a fixed astrometric grid and stacking of the swarped images. However, the pipeline was originally designed to deal with high-galactic latitude fields and for a completely different observing strategy than the one adopted for the present survey. In particular, the fact that the number of dithered images is small and the fields are crowded required some changes in the reduction strategy. As discussed below, the results also showed the need for additional modifications of the software, which are currently under way. One of the issues not addressed in the present paper is the procedure required for de-fringing the I-band images for which the solution adopted for the Deep Survey is not applicable to the present observations. It is important to emphasize that the I-filter in use is very red compared to the standard Cousins, with a broad spectral coverage to the red. Tests have also shown the fringing pattern to be variable during the course of one night. Methods for dealing with the fringing and the impact of its removal will be discussed in a subsequent paper.

4. Astrometry

As mentioned above, a key issue of concern regarding the PF survey is the astrometric calibration of the images and of the target lists which will be used for FLAMES observations. In this section, the algorithm used in the calibration of the images and an evaluation of the available reference catalogs are discussed.

The astrometric calibration performed by the EIS pipeline makes extensive use of the method developed by Djamdji et al. (1993) based on the multi-resolution decomposition of images using wavelet transforms. As described in Arnouts et al. (2001), this package is used both to obtain a crude first estimate of a suitable reference pixel for

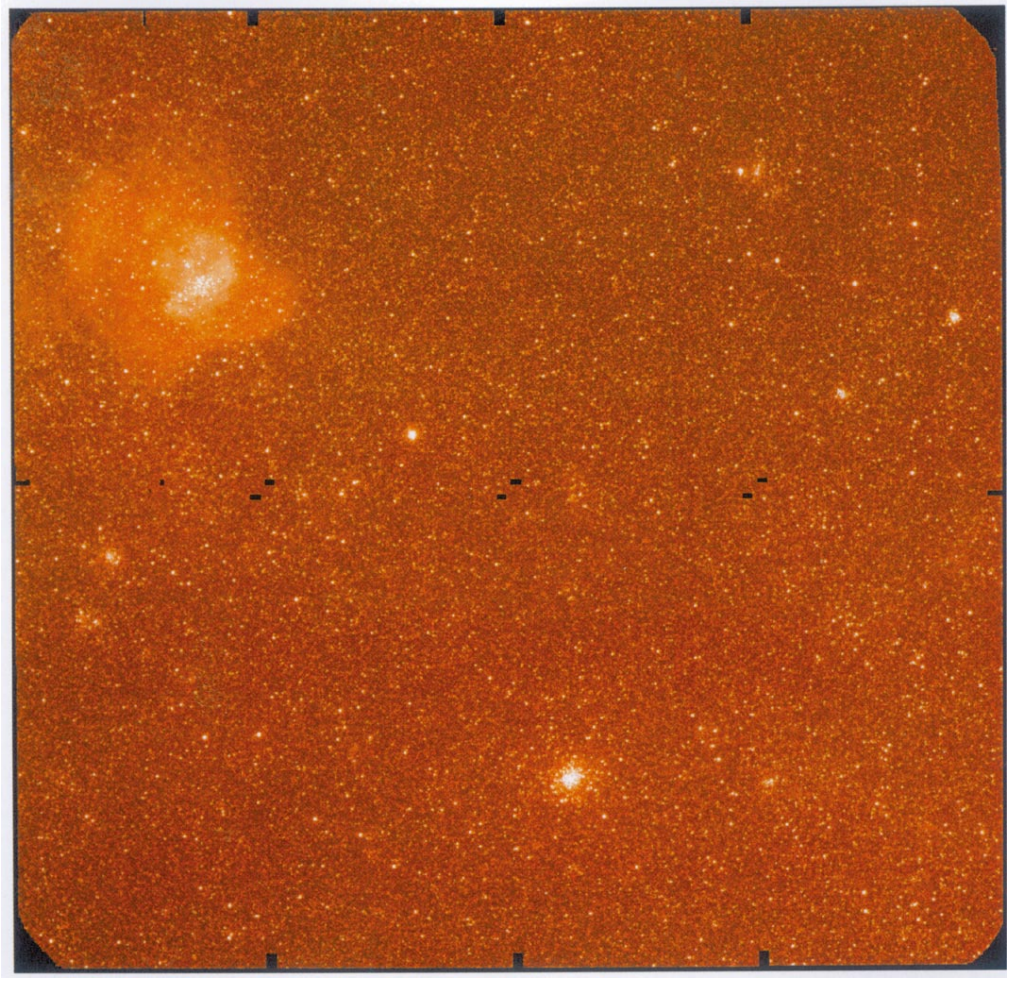

Fig. 1. The V band of the SMC 5 field covering a field of view of 34×33 arcmin. This image is the combination of the two DEEP dithered images. The small black areas seen along the central part of the image and at the edges are the residuals of the inter-chip gaps. In this field the following clusters are present: NGC 346 (the brightest HII region in the SMC), NGC 330, IC 1611, NGC 306, NGC 299, OGLE 109, OGLE 119, OGLE 99.

the WFI images for the run, and an accurate determination of the astrometric solution for each image. Once an adequate reference pixel is available for the run, the science images are decomposed into images of different resolutions. The same is done for a mock image created from the positions of stars taken from the reference catalog being used. The lowest resolution images obtained are then correlated and a first approximation of the astrometric solution, in this case a translation, is determined. This solution is then used to correct the positions of the source catalog extracted from the next higher resolution science image. The source catalog is extracted using a simple algorithm which identified local maxima. This procedure is then repeated for each subsequent resolution, while the search radius used to identify matching objects decreased. At the highest resolution a polynomial of second-order is used and the search radius is half a pixel, which in the case of WFI corresponds to ∼0.14 arcsec.

Once an astrometric solution is found for each CCD of the mosaic, the image is then corrected for distortions by swarping it using a *nearest neighbor* criterion to relocate the flux. While this proved to be adequate for the DPS survey, the results of tests discussed below show that this strategy has to be modified for the PF survey due to the small number of images per pointing. In this case, it is necessary to re-sample the images by factors of two and three to obtain the best results. This re-sampling strategy has been adopted as a temporary solution. A more general swarping technique is currently being implemented into the pipeline which will allow for a suite of kernels to be chosen. This technique and their impact on the astrometric calibration will be discussed in a subsequent paper of this series.

After the registration of the individual images, a final combined image can be produced by simply adding the two images using the weight image to eliminate cosmic rays and bad pixels. As an illustration, Fig. 1 shows the final V-band image of the SMC 5 field covering 34× 33 arcmin. The observing strategy adopted leads to a filling factor of 99.91%, albeit with regions less sensitive than others. Note, however, that the imprints of the gaps are not completely removed and can still be seen aligned along

the central part of the image and at the edges. It is interesting to note the large number of stellar systems that can be seen in this field, among them: NGC 346, NGC 330, IC 1611, NGC 306, NGC 299, OGLE 109, OGLE 119, OGLE 99.

Considering the importance of an accurate astrometric solution in the preparation of target lists for any fiber system, such as FLAMES, several tests were performed in order to evaluate and fine-tune the "swarp" algorithm and to chose the best reference catalog. These tests were conducted using the data for the nearby open cluster M 67 (EIS target OC99), for which results of several previous work are available in the literature. For instance, the work of Girard et al. (1989) provides a source catalog with positions having a typical internal relative error of $\simeq$0.021 arcsec for a sample of 663 stars, with errors of $\simeq$0.010 arcsec for the stars with $V < 14$. Their estimated external (absolute) error is 0.16 arcsec. The catalog also gives proper motions measurements for each star for a mean reference epoch of 1950.8.

4.1. Fine-tuning the pipeline

A first set of tests were carried out to establish the best re-sampling strategy to be used in the astrometric calibration of the images. First, the SHALLOW and DEEP images of OC 99 were astrometrically calibrated using the nearest neighbor algorithm without image re-sampling, the default mode of the pipeline. Second, the photometric pipeline (see Sect. 5) was run to extract point-like objects and construct catalogs for both the SHALLOW and the combined DEEP images. The reader is reminded that the SHALLOW and DEEP images were astrometrically calibrated separately and thus have independent solutions. The upper panel of Fig. 2 (panel A) shows a comparison between the derived SHALLOW and DEEP catalogs. From the figure, one can clearly see the undesirable effect of the nearest neighbor approach. In this case, the distribution of the positional residuals in RA and Dec are highly non-Gaussian, with the residuals in RA being described by a bi-modal distribution with the peaks separated by $\sim$0.24 arcsec, corresponding to one WFI pixel. This systematic effect is an artifact introduced by the nearest neighbor approach without image re-sampling. This effect becomes obvious when one is dealing with a small number of images, as in the present case. Better results are obtained when the image is re-sampled and each original pixel is split into 2×2 pixels. This case is shown in the middle panel of Fig. 2 (panel B), where the peaks of the bi-modal distribution are much closer together and the distribution of the residuals resembles more closely that of a Gaussian. Even better results are obtained using a higher resolution re-sampling with each pixel being split into 3×3 pixels. This is shown in the lower panel of the same figure (panel C). The latter sampling leads to a Gaussian distribution with an rms of $\simeq$0.05 arcsec in both coordinates. For all three cases the variation of the RA and Dec

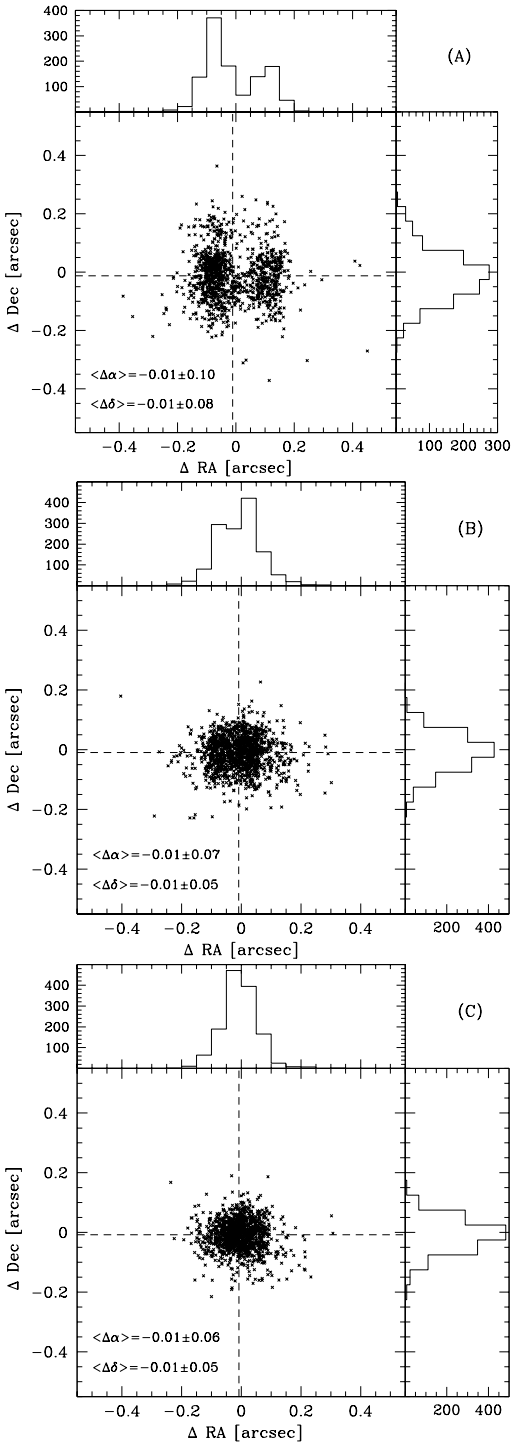

Fig. 2. Comparison of the two independent astrometric calibration of the SHALLOW and DEEP exposures adopting the USNO catalogue for the field of M 67 (OC99). **A)** Nearest neighbor algorithm with sub-sampling of 1×1. **B)** Same as above but with pixel sub-sampling of 2×2. **C)** Same as above but with pixel sub-sampling of 3×3. The vertical and horizontal dashed lines mark the mean residuals in RA and Dec after applying a 3σ clipping to the data. The mean values with the final $1 \times \sigma$ rms are given on the figure. Also shown are the histograms of the residuals as a function of RA (top) and Dec (right).

residuals as a function of magnitude were inspected and were found to be negligible. Note that while the mean offset of the residuals do not change, the rms is significantly smaller in the right ascension direction between the first and last cases.

The results of these tests show that in order to avoid systematic errors between bright and faint sources a re-sampling of the image is required if the nearest neighbor strategy is adopted. In this paper, all images have been re-sampled by splitting the original pixels in 3× 3 sub-pixels. However, since re-sampling the image is costly in processing time, a more general swarping algorithm has been developed to avoid the discreteness effects of the nearest neighbor approach. This algorithm is currently being implemented into the EIS pipeline. It will be used for all subsequent reductions of the PF survey data.

4.2. Choice of the reference catalog

Another important issue to consider is the impact of the reference catalog used. In order to evaluate the available catalogs, the amplitude of the residuals, their dependence on position and on apparent magnitude, and their comparison with an independent astrometric catalog are investigated in this section. It is important to point out that during the analysis of the data presented in this paper only two reference catalogs were available – the USNO 2.0 and the GSC 2.1, a pre-release version of the Guide Star Catalog version 2, used as the reference catalog in the most recent EIS reductions (e.g. Vandame et al. 2001; Arnouts et al. 2001). However, right before the release of these data, the GSC 2.2 version (McLean et al. 2001) became available. While it was not possible to re-analyze all of the data in time for the scheduled release, the GSC 2.2 was used in the tests presented here to assess the differences, if any, relative to the pre-release version. This is important because at the time of writing a number of fields observed as part of the PF were not yet covered by the GSC 2.2. This raised the issue of whether the GSC 2.1 or the USNO 2.0 should be used for the first PF release.

In the present analysis, the SHALLOW images of M 67 were calibrated using the three reference catalogs described above. Next, the positional differences between the calibrated source list and the reference catalog were computed. The RA and Dec residuals are shown in Fig. 3 for each reference used. For consistency, only objects brighter than $m = 18.5$ are plotted, this lower limit corresponding to the magnitude cutoff of the GSC 2.2 catalog. From the figure, one can immediately see the superiority of the GSC 2.2 relative to the other catalogs considered. The distribution of the residuals using the GSC 2.2 catalog is highly concentrated and Gaussian in both directions. This is in marked contrast to the other two which have a much wider spread in the ΔRA–ΔDec plane, and either very skewed (USNO 2.0) or bi-modal (GSC 2.1) distributions. The mean offsets and the rms of the distributions, given on each panel, show that while the systematics of the USNO 2.0 and GSC 2.1 may be different, which could be partly due to the different epoch of the photographic

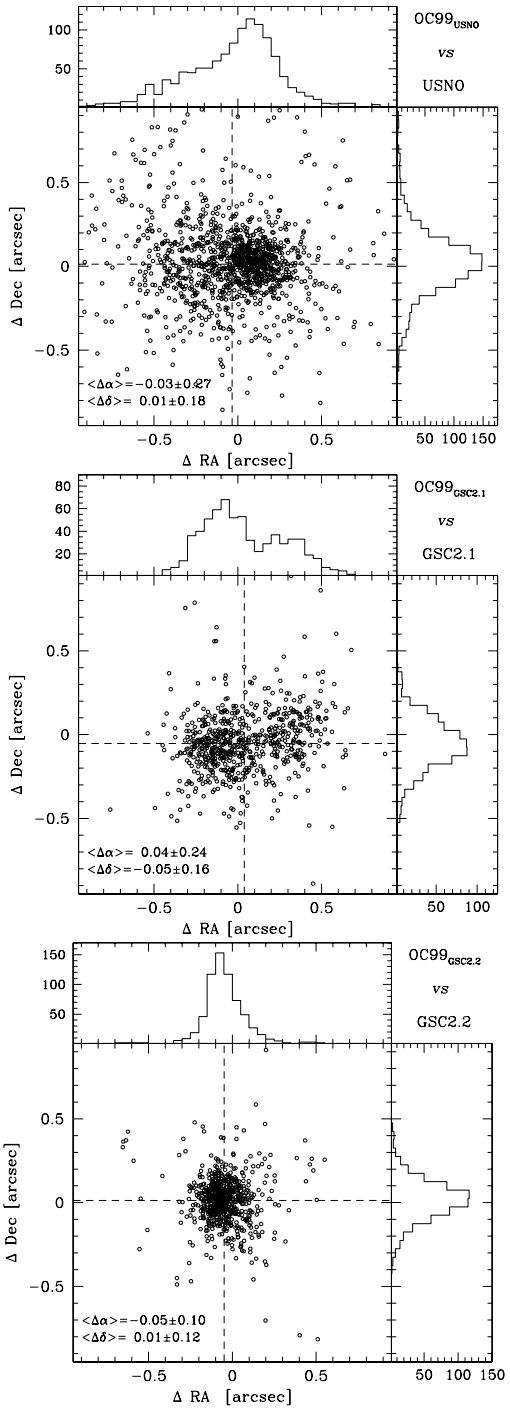

Fig. 3. The two-dimensional (RA, Dec) distribution of positional residuals obtained from the comparison of the astrometrically calibrated SHALLOW catalogs of M 67, using different reference catalogs, and the reference catalog used: USNO 2.0 (upper panel); GSC 2.1 (middle panel); and GSC 2.2 (lower panel). The vertical and horizontal dashed lines mark the mean residuals in RA and Dec after applying a 3σ clipping to the data. The mean values with the final $1 \times \sigma$ rms are given in the figure. Also shown are the histograms of the residuals as a function of RA (top) and Dec (right).

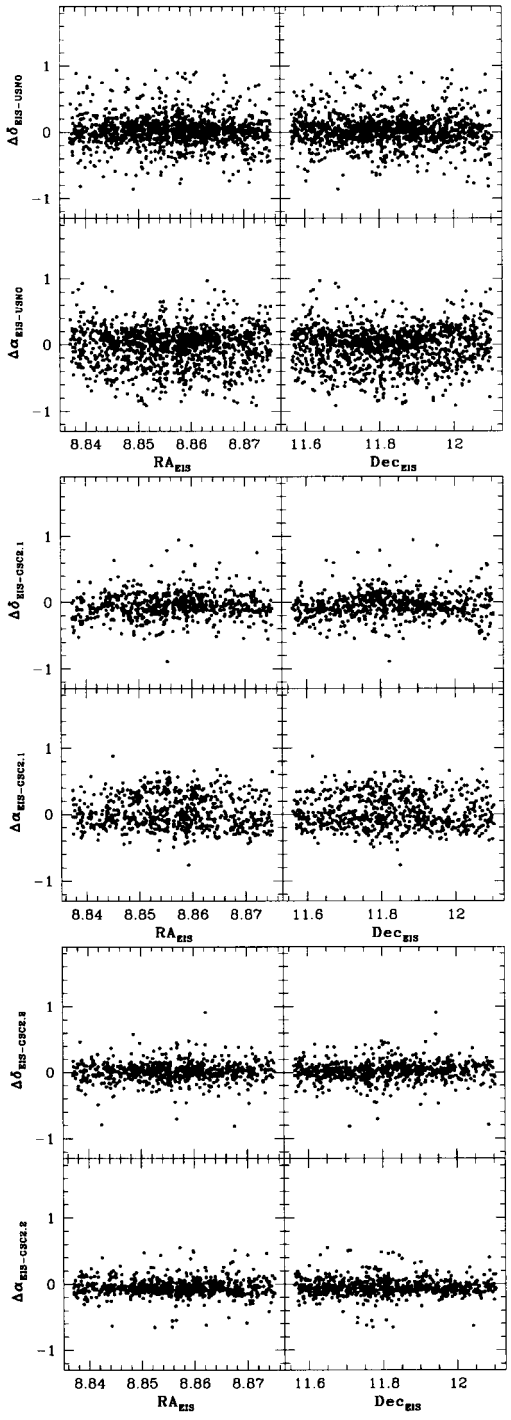

Fig. 4. The positional residuals in RA and Dec computed as in Fig. 3, are shown as a function of RA and Dec of the EIS catalog positions for the USNO 2.0 (upper panel); GSC 2.1 (middle panel); and GSC 2.2 (lower panel).

plates, both have comparable accuracy (∼0.25 arcsec), as measured by the rms of the distribution. On the other hand, GSC 2.2 represents a real improvement with the rms of the residuals being $\lesssim$0.12 arcsec.

To understand the nature of the observed spread of the residuals, the Δ RA and Δ Dec residuals are plotted as a function of RA and Dec taken from the calibrated EIS catalogs. This is shown in Fig. 4 and for each of the considered catalogs. In general, besides the large scatter, no noticeable systematics are seen. Note, however, the two bands of data points seen in the GSC 2.1 residuals, the reason for which is discussed below. It is worth pointing out that while no correlation between the residuals and position were found, other than that previously mentioned, for the particular field considered here, GSC 2.1 did show a systematic variation of the residuals as a function of both RA and Dec in the case of the Chandra Deep Field south located at the edge of the plate (Arnouts et al. 2001). It remains to be seen if this effect has been corrected for in the GSC 2.2.

Table 2. Linear fit parameters for the positional residuals as a function magnitude.

Catalog	Residual	slope	zero-point	rms
USNO	Δ RA	−0.046	0.684	0.262
USNO	Δ Dec	0.011	−0.149	0.232
GSC 2.1	Δ RA	−0.009	0.388	0.180
GSC 2.1	Δ Dec	−0.019	0.248	0.205
GSC 2.2	Δ RA	0.014	−0.268	0.128
GSC 2.2	Δ Dec	−0.024	0.381	0.139

* Only objects brighter than 14.8.

Complementing the above plots, Fig. 5 shows the variation of the right ascension and declination residuals as a function of magnitude for the USNO 2.0 (top panel), GSC 2.1 (middle panel) and GSC 2.2 (bottom panel). Also shown is the linear fit to the residuals as function of magnitude. The fit parameters are given in Table 2. From the figures and the table, one finds a relative strong dependence of the residuals on the magnitude for the USNO 2.0 and a striking discontinuity at $m \sim 15$ in the GSC 2.1. Only GSC 2.2 shows no systematic behavior with magnitude. From the liner fit of the USNO residuals one finds an offset in the RA residuals of ∼0.30 arcsec between bright and faint stars ($12 < V < 18.5$). The effect in Dec computed over the same magnitude interval is negligible. This systematic error is large compared to the required accuracy of the relative positions. This offset is significantly smaller in the case of GSC 2.2, being $\lesssim$0.10, in both directions. The systematic variation of the residuals with the magnitude explains the amorphous distribution seen in Fig. 3. This magnitude dependence has no bearing on the astrometric calibration of the pipeline. Note that this means that one should not use the coordinates of a reference star as listed in the reference catalog. Instead, stars used for pre-setting the telescope must share the same astrometric system as the objects being observed.

As an external check of the different astrometric solutions obtained for M 67, these were compared with the astrometric catalog of Girard et al. (1989). In this

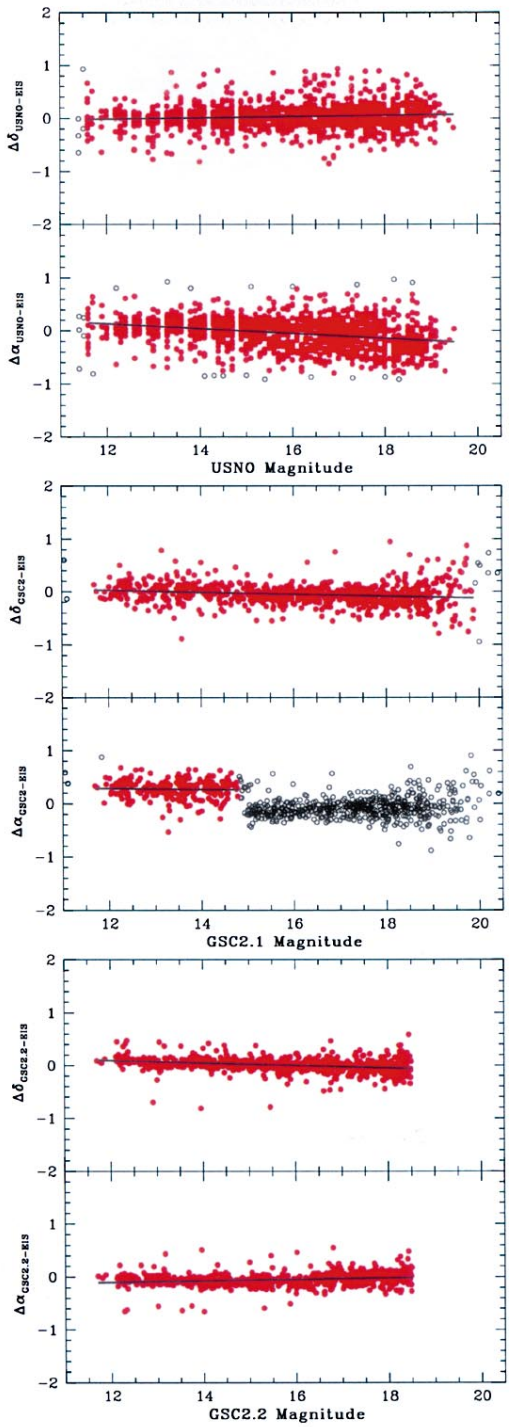

Fig. 5. The positional residuals in RA and Dec computed as in Fig. 3, shown as a function of the magnitude listed in the respective reference catalogs used for the USNO 2.0 (upper panel); GSC 2.1 (middle panel); and GSC 2.2 (lower panel). Points represented by filled circles were used in the linear fit to the data. The fit parameters are listed in Table 6.

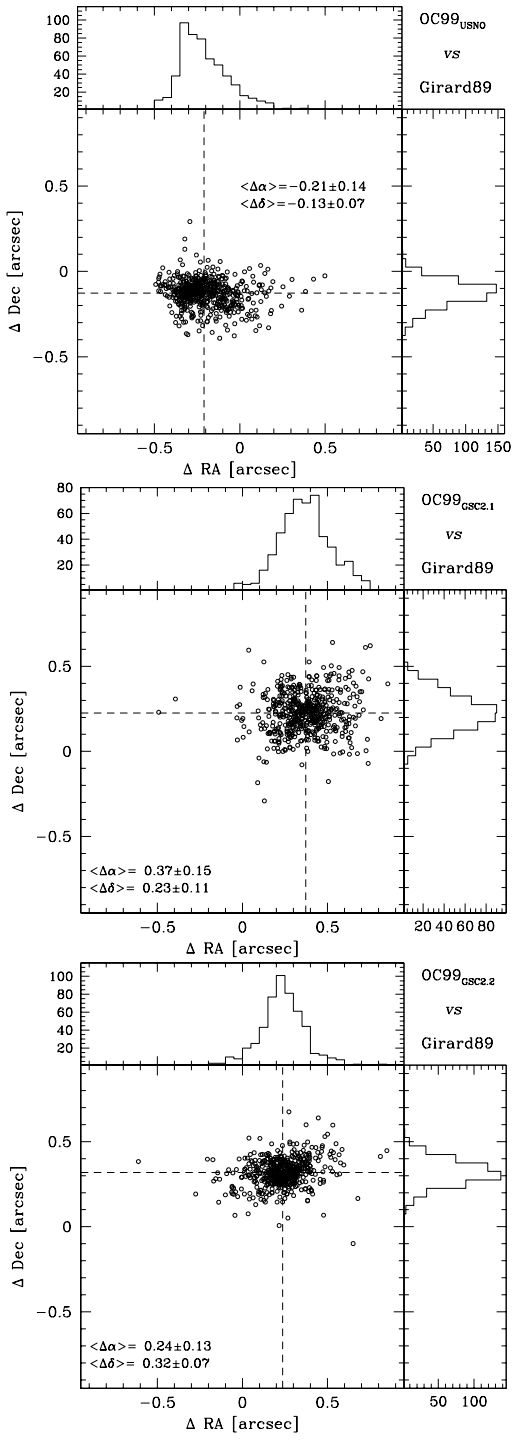

Fig. 6. The two-dimensional (RA, Dec) distribution of positional residuals obtained from the comparison of the astrometrically calibrated catalogs of M 67, using different reference catalogs, with the astrometric catalog of Girard et al. (1989). The EIS catalogs were calibrated astrometrically adopting: USNO 2.0 (upper panel); GSC 2.1 (middle panel); and GSC 2.2 (lower panel). The vertical and horizontal dashed lines mark the mean residuals in RA and Dec after applying a 3σ clipping to the data. The mean values with the final $1 \times \sigma$ rms are given in the figure. Also shown are the histograms of the residuals as a function of RA (top) and Dec (right).

comparison, the position of the stars in the Girard et al. catalog were corrected for proper motion to the PF epoch of observation. The distribution of the positional residuals in the RA–Dec plane are shown in Fig. 6 for the EIS

catalog produced for M 67 field using USNO 2.0 (top panel), GSC 2.1 (middle panel) and GSC 2.2 (bottom panel). Also shown in the figure are the distributions of the residuals in the RA and Dec directions. In each panel the mean offset and rms, computed after applying a 3σ clipping to the data, are also shown. While the rms values obtained are comparable ($\lesssim$0.15 arcsec), only for GSC 2.2 are the residuals well represented by a Gaussian distribution. Note that the mean offsets are not relevant for the preparation of target lists for FLAMES since its fiber positioner is allowed to move within a 2 arcsec window (Pasquini, private communication).

In conclusion, an analysis of the three reference catalogs currently available for the astrometric calibration of the WFI images shows that the recently released GSC 2.2 catalog yields the best results overall, with less systematics than the USNO 2.0 current in use by EIS. The analysis also reveals some unexpected features of the GSC 2.1 used in the calibration of the Chandra Deep Field south (EIS DEEP 2c field; Arnouts et al. 2001), pointing out the need for a re-evaluation of the astrometric calibration of those images. Nevertheless, it is important to emphasize that in all cases the rms of the residuals are below the 0.2 arcsec upper-limit required for the optimal performance of FLAMES. Since at the time of writing the GSC 2.2 catalog did not cover the SMC fields presented in this paper, the USNO 2.0 was used as the reference catalog. However, the results presented in this section clearly suggest that the GSC 2.2 reference catalog shows no significant systematic errors and is currently the best available. Future EIS calibrations will be done using this catalog, as soon as all the fields of interest are available. The results also demonstrate that the algorithm being employed in the astrometric calibration of the WFI frames in the EIS pipeline is robust, yielding results within the requirements of FLAMES. One also finds that the accuracy of the astrometric solution is limited by the intrinsic errors of the reference catalog used.

5. Photometry

5.1. Source extraction

Source extraction and stellar photometry (PSF fitting technique) were performed using the DAOPHOT/ALLSTAR package (Stetson 1987). Minor changes to these programs had to be made to enable them to read fits images directly and to handle 8k×8k images, which basically required increasing the memory buffer, the size of the buffer used for determining the sky level and the number of stars used to model the PSF function for a frame. In addition, a number of procedures were implemented to automatize the whole procedure and make it more adaptable to the pipeline framework.

The first step is to create a model PSF for each image. The building of the PSF for each frame was done iteratively using a set of isolated and unsaturated stars. A preliminary list typically containing 500 stars is extracted and a first rough PSF is generated. Objects with poor fits are discarded from the list and a new PSF is created. This process is repeated until the fitting solution is acceptable for all objects. Typically, the process converges after a few iterations with the final PSF determined by at least 300 stars per image. The final model for the PSF is generated with a "Penny" function which has a quadratic radial dependence on the stellar coordinates. The resulting PSF is then used by the ALLSTAR routine to measure the magnitudes of all point sources detected by the FIND command of DAOPHOT. The final star-subtracted image is then visually inspected to check the result.

The above procedure was used to produce stellar catalogs for the SHALLOW and DEEP images of all selected fields in B and V. The catalogs extracted from the combined DEEP images are very sensitive to the detection threshold used. In all cases, the detection threshold was set to 3σ above the background counts, the best compromise between completeness and the number of spurious detections. Lower thresholds cause a large increase in the number of spurious objects. This is especially true for the DEEP images which have a lower signal-to-noise at the edges and over regions sampled by a single image due to the inter-chip gaps. This means that some faint objects within these regions might be missed. Information regarding the location of these regions can be found in the corresponding weight-maps (see Sect. 6).

Since the DAOPHOT/ALLSTAR package only works in pixel coordinates, the astrometric calibration available in the header of the image being processed is used to transform the resulting catalog to the world-coordinate system (*wcs*). This is in contrast to the procedure adopted by the EIS pipeline, which normally uses SExtractor which supports the *wcs* convention. Once catalogs from the SHALLOW and DEEP images are available those in the same passband are matched and the magnitude of objects in the SHALLOW catalogs are scaled to those in the DEEP catalogs. In the process the error weighted mean of the magnitude differences is computed for the stars in common, which never exceed 0.03 mag. It is important to point out that the SHALLOW and DEEP images overlap over an interval of 6 mag. The SHALLOW and DEEP catalogs are then merged and only objects satisfying the conditions $CHI < 1.2$ and $-1.2 < SHARP < 1.2$ are kept in the final combined catalog. The parameters CHI and $SHARP$ are a measure of the quality of the PSF fitting and the sharpness of the light profile of the object, respectively. Their exact definition can be found in the documentation of the DAOPHOT/ALLSTAR package. Finally, a BV color catalog is produced by associating the entries of the combined single passband catalogs described above, using a matching radius of 0.8 arcsec. The color catalogs also include objects detected in only one passband to avoid discarding intrinsically "blue" or "red" stars. The instrumental PSF magnitudes are then aperture-corrected and calibrated as described in the next section.

Table 3. Total number of sources in the released BV catalogs.

Name	EIS name	Number
Berkeley 20	OC03	7190
NGC 2477	OC12	38800
NGC 2506	OC14	18900
Messier 67	OC99	4290
SMC	SMC 5	280000
SMC	SMC 6	246000

5.2. Photometric calibration

The images were calibrated to the Johnson-Cousins system using observations of Landolt (1992) standard stars. Photometric solutions were determined using mean extinction coefficients and empirically determined color terms given by the equations:

$$B_{\rm JC} = B_{\rm EIS-842} + 0.29 \times (B-V)_{\rm JC} \quad (1)$$

$$V_{\rm JC} = V_{\rm EIS-843} - 0.08 \times (B-V)_{\rm JC} \quad (2)$$

where $B_{\rm EIS-842}$ and $V_{\rm EIS-843}$ are in the EIS magnitude system, and the numbers correspond to ESO's filter identification number. The extinction coefficients for each passband were computed from the mean extinction curve for La Silla and the response of the WFI filters used yielding: $K_B = 0.235$ and $K_V = 0.135$.

The instrumental PSF magnitudes were converted into aperture magnitudes, assuming that $m_{\rm ap} = m_{\rm PSF} +$ constant (Stetson 1987), where the constant is the aperture correction. This was obtained for each image from the analysis of the growth curves of bright isolated stars identified on each frame. Typical values for the aperture correction are in the range 0.15–0.3 mag. In the case of crowded regions, like the SMC fields, aperture corrections were calculated after subtracting all stars around the measured bright objects.

As an example of the application of the above procedure, Fig. 7 shows the color-magnitude diagram obtained for the SHALLOW (top panel) and the DEEP (bottom panel) color catalogs. Note that the color-magnitude diagram derived from the SHALLOW catalog extends from V 10 to $V \sim 20$, while that derived from the DEEP catalog covers the magnitude interval $14 \lesssim V \lesssim 23$. The color-magnitude diagram of the final merged catalog covers an impressive 13 mag interval, as shown in Figs. 9 and 10.

The number of objects given in the final BV color catalog for each field is listed in Table 3. The table gives: in Col. (1) the name of the primary target; in Col. (2) the EIS identification name; and (3) the total number of sources.

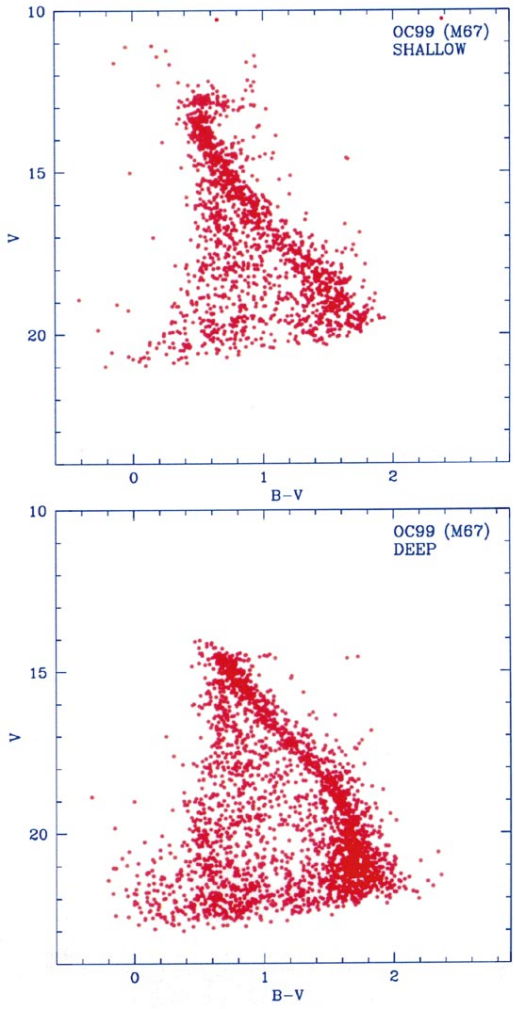

Fig. 7. The M 67 (OC99) color-magnitude diagram obtained from the final combination of the SHALLOW and DEEP data.

5.3. Comparison with other authors

As a check of the photometric catalogs being produced, these are compared to the data from Montgomery et al. (1993) for M 67 (OC99) and Vallenari et al. (1994) for NGC 330 (SMC5). The results of these comparisons are shown in Fig. 8. The two sets of panels refer to M 67 and NGC 330, respectively. In these plots the differences in the $(B-V)$ color (upper plot) and in the V magnitude (lower plot) are displayed as a function of the EIS V Johnson-Cousins magnitude. In these plots all stars in common are included.

For M 67 one finds a mean offset in the photometric zero-point of 0.068 mag and an rms of 0.064 mag in the magnitude interval $10 < V < 20$. For the $(B-V)$ color one finds a mean offset of -0.017 mag and an rms of 0.11 mag. In the case of NGC 330, one finds a mean value of magnitude differences of 0.050 mag, similar to the one mentioned above, and an rms of 0.18 mag, while the mean offset in $(B-V)$ is 0.053 mag with an rms of 0.15 mag, in the same magnitude interval as for M 67. Together, these results show that the measured colors are in excellent agreement

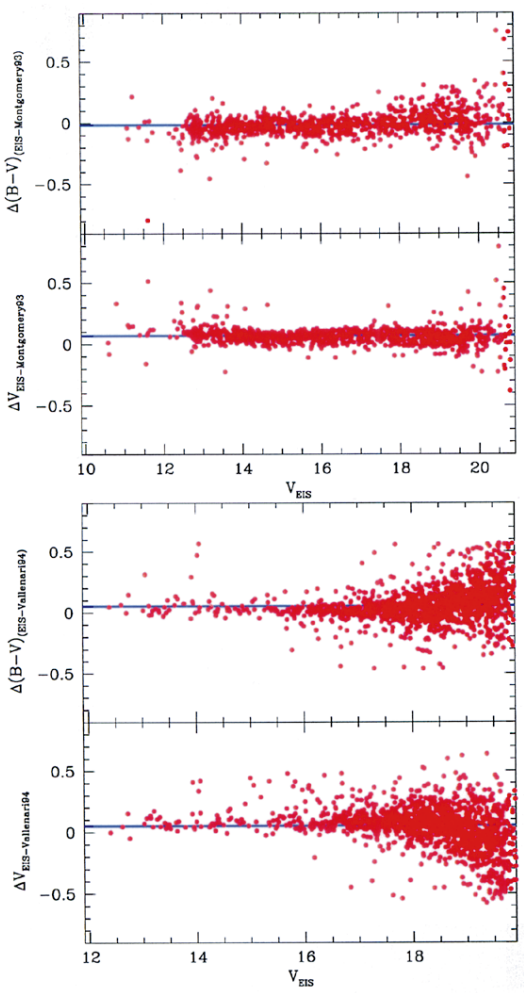

Fig. 8. Magnitude and color comparison of the EIS catalog with other authors. The *upper panel* shows a comparison of the EIS photometry of the M 67 (OC 99) field with that of Montgomery et al. (1993). The $(B-V)$ and V residuals are plotted against EIS V calibrated magnitudes. The *lower panel* shows a similar comparison but for NGC 330 (SMC 5) with the Vallenari et al. (1994). In these plots the horizontal lines indicate the median value of the differences.

with those measured by other authors despite of the large color term involved in the correction of the WFI instrumental magnitudes to the Johnson-Cousins system. The results also show that the present data may have a systematic error of $\lesssim$0.07 mag in the zero-point, which should be further investigated. More importantly, if one assumes that the random errors for EIS and the Montgomery et al. data are comparable, then the measured rms of the magnitude differences for M 67 implies an error of ∼0.04 mag at $V \sim 20$ in the EIS catalogs. This value is consistent with the internal estimates and the original requirements for the PF survey. The larger scatter measured from the comparison of NGC 330 may be due to the larger uncertainties in the magnitudes due de-blending problems in such very dense system.

6. Survey products

The images already released include the combined deep B and V exposures of each field, with all images normalized to 1 s exposure, and are presented in the TAN projection. In the data release the science images have been combined with their corresponding weight-maps into a single fits file containing two image extensions.

In addition to the pixel maps, for each of the six observed fields discussed in this paper, the following catalogs are also available:

1. Three instrumental photometric catalogs for each passband: the SHALLOW, the DEEP and the combined catalog, all in ASCII format. The following naming convention is adopted

   FIELD_FX_N_YYYY-MM-DDTHH:MM:SS.asc

   where FIELD is EIS target name, FX is the passband, N varies from 1 to 3 and corresponds to the SHALLOW, DEEP and COMBINED catalogs, respectively. The remaining characters refer to the date and time of the catalog production.
2. A calibrated BV color catalog available in three different formats for the convenience of the interested user: a FLAMES input file `.fld`, a SKYCAT input file `.scat`, and a normal ASCII file `.asc`. The name of each file follows the convention described above.

An example of the FLAMES input `.fld` file is shown in Table 4. The first four rows of the file are part of a header which includes: a LABEL with the name of the field; the UTDATE of the observations (this have to be changed according to the needs of the user); the CENTER of the field in RA and Dec coordinates; the EQUINOX of the coordinates (in this case, J2000.0). The targets following the header have the following fields: in Col. (1) the identification sequential number; in Cols. (2)–(4) the RA of the object in hours; in Cols. (5)–(7) the declination of the object in degrees; in Col. (8) one letter specifying the kind of fibers to be used among the different types available (e.g. FLAMES in MEDUSA mode is be identified with the "P" letter); in Col. (9) observation priority of the objects (highest 1; lowest 9), in this example, 1 is given for all the object; in Col. (10) measured V magnitude of the object; in Col. (11) another identification code (0 in this example); and in Col. (12) a comment field, which in this example lists the $(B-V)$ color.

7. Discussion

7.1. Color-magnitude diagrams

In order to illustrate the results obtained from the photometric data presented here, Figs. 9 and 10 show the color-magnitude diagram (CMD) for each of the observed fields. For most fields the CMDs were obtained using the catalog within the entire area covered by WFI. However, and in order to minimize foreground/background contamination, for the open clusters Berkeley 20 and NGC 2506,

Table 4. An example of a FLAMES operating system input file (.fld).

Header	LABEL EIS PF FIELD OC99							
	UTDATE 2001 07 01							
	CENTER 08 51 23.073 11 50 7.83							
	*EQUINOX J2000.0							
Targets								
	OC99_000001	08 50 26.850	11 33 43.03	P	1	16.620	0	1.663
	OC99_000002	08 52 04.271	11 33 49.17	P	1	18.292	0	1.509
	OC99_000003	08 51 01.327	11 33 50.11	P	1	19.078	0	0.829
	OC99_000004	08 51 10.555	11 33 53.43	P	1	17.743	0	1.219
	OC99_000005	08 51 40.304	11 33 55.29	P	1	17.299	0	0.885
	OC99_000006	08 50 19.500	11 33 58.38	P	1	19.069	0	1.460
	OC99_000007	08 50 26.126	11 33 59.22	P	1	18.705	0	1.049
	OC99_000008	08 50 28.017	11 34 01.92	P	1	20.661	0	1.506
	OC99_000009	08 52 05.010	11 34 08.15	P	1	18.423	0	1.515

the CMDs shown correspond to a circular region around the nominal cluster center of 3 and 5 arcmin in radius, respectively.

Even though still a small sample, the examples presented here show the large variety of stellar systems being observed by the PF survey in terms of age, metallicity, size, distance and environment. The wide-area and the extended magnitude coverage (∼13 mag) down to $V \sim 23$ provide an invaluable data set to extract samples suitable for the scientific drivers of FLAMES which include, among others, studies of: chemical abundances of stars in clusters and selected galactic regions (Bulge, Disk, and Halo); stellar kinematics and structure of stellar clusters; chemical composition and dynamics of nearby dwarf spheroidal galaxies; circumstellar activity in young stellar objects; very low mass stars and brown dwarfs in star forming regions.

From Figs. 9 and 10 one can see systems with well-defined main-sequences (MS), probable binary sequences, blue straggler populations, red clump stars, potential white dwarf candidates, very red objects and systems with composite stellar populations including very young stellar associations, and additional information about the galactic structure. These points are briefly discussed on an individual basis below.

7.2. Comments on individual systems

7.2.1. M 67

The close location to the Sun ($(m - M_V) = 9.59$), the low reddening, ($E_{B-V} = 0.05$; Montgomery et al. 1993), the rich population (800 $M_\odot$; Mathieu 1985; Montgomery et al. 1993) and the minimum contamination by foreground/background stars make M 67 one of the best studied open clusters. By fitting theoretical isochrones to the observed MS, Dinescu et al. (1995) derived an age of 4.0 ± 0.5 Gyr. Tautvaisiene et al. (2000) estimated a mean metallicity of [Fe/H] $= -0.03 \pm 0.03$. This system is also of great interest because of its rich population of blue-stragglers, X-ray sources and white dwarfs. In many ways, M 67 is an ideal case for studies of the structure and evolution of Population I stars and thus a prime target for a spectroscopic follow-up with FLAMES. Moreover, and thanks to the precise proper-motions study of 663 stars by Girard et al. (1989), M 67 has been used as a test case for the astrometric calibration procedures adopted in the reduction of the PF data (Sect. 4).

From the CMD shown in Fig. 9, the MS is clearly discernible from the cluster turnoff (TO) at $V \simeq 12.8$ down to $V \simeq 22$. At $V \sim 18.5$ the MS shows an abrupt change in slope. At fainter magnitudes the $(B - V)$ is almost constant ($\simeq$1.8) due to the saturation of this color for very cool stars, corresponding to $M \sim 0.5\ M_\odot$. This may be also caused by a strong contamination by background stars and galaxies at the very faint end of the MS. The large magnitude baseline of the CMD allows allows one to probe the red giant branch up to $V \sim 10.0$. One can also see several blue stragglers at magnitudes brighter than $V = 12.5$ and in the color interval $-0.6 < (B - V) < 0.8$.

Close inspection of the CMD suggests the presence of a sparse, redder sequence running parallel to the cluster main sequence, as seen by Montgomery et al. using BVI data (see also Sect. 7.3). This has been interpreted as due to binary systems, estimated to constitute 38% of the cluster population. Furthermore, Pasquini & Belloni (1998), based on photometric and high-resolution spectroscopic studies of ROSAT sources, concluded that most of the detected X-ray sources are binaries. These ROSAT sources have peculiar locations in the cluster CMD consistent with the above interpretation.

Finally, several blue objects ($(B-V) < 0.4$) are visible fainter than $V \simeq 19$. These objects could be the brightest members of the white dwarf (WD) cooling sequence found by Richer et al. (1998), in the absolute magnitude interval of $M_V = 10-14.6$.

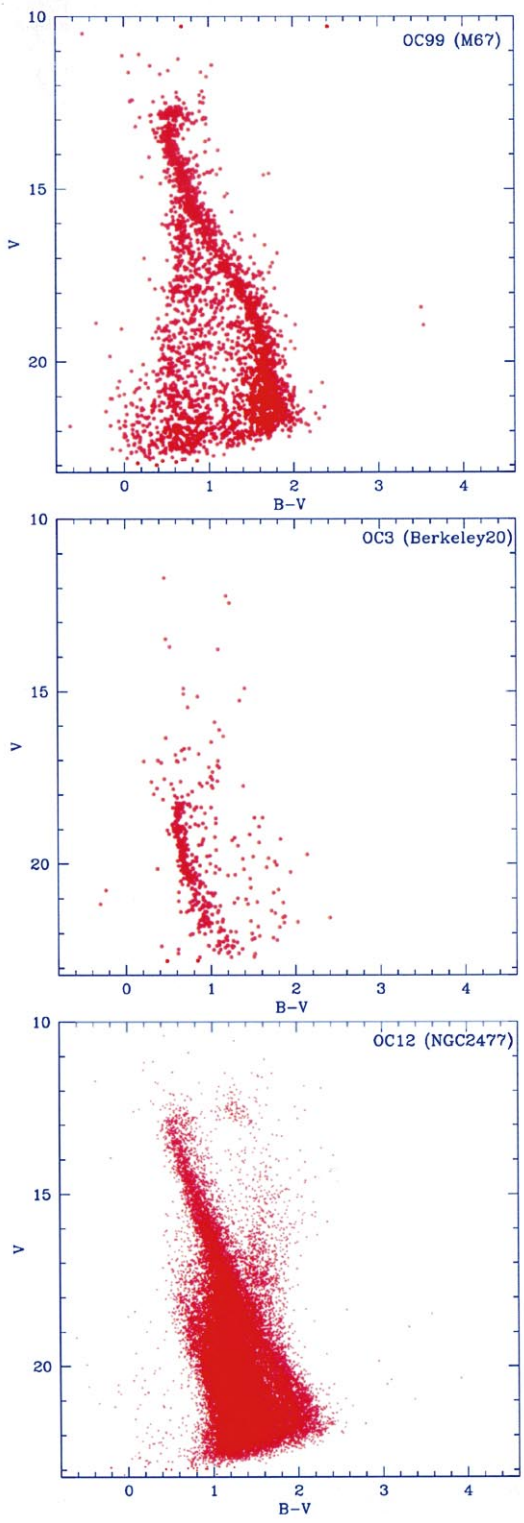

Fig. 9. The CMD for M 67, Berkeley 20 and NGC 2477, obtained from the combination of the catalogs extracted from the SHALLOW and DEEP images, as described in the text. To minimize foreground contamination the CMDs of Berkeley 20 corresponds to circular regions of 3 arcmin in radius around the nominal center of the cluster.

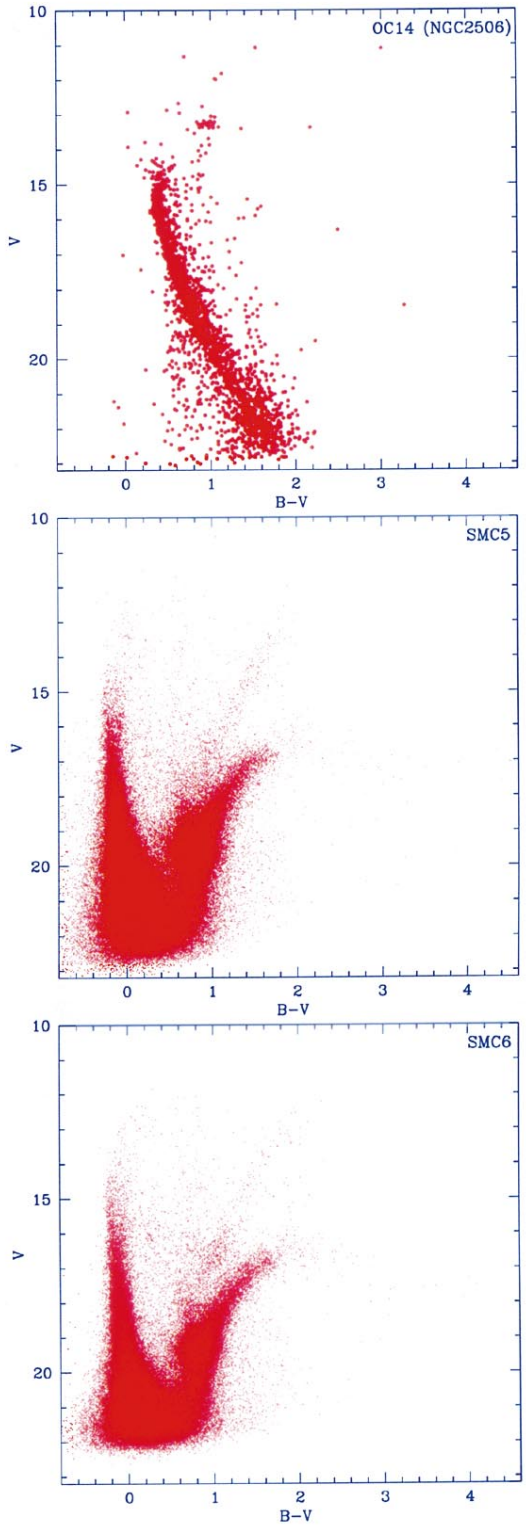

Fig. 10. The CMD for NGC 2506, SMC 5 and SMC 6, obtained from the combination of the catalogs extracted from the SHALLOW and DEEP images, as described in the text. To minimize foreground contamination the CMDs of NGC 2506 corresponds to circular regions of 5 arcmin in radius around the nominal center of the cluster.

7.2.2. Berkeley 20

From the study of several stellar systems carried out by Phelps et al. (1994), Berkeley 20 is ranked as one of the oldest open clusters, with an age comparable to that of M 67. From an analysis of the $V-(V-I)$ CMD

MacMinn et al. (1994) estimate a mean age of 6 Gyr and a metallicity of [Fe/H] $\simeq -0.23$. However, the system is further away, with a distance modulus of $(m-M)_V \simeq 15.0$ mag. It is also located in a direction of higher extinction, estimated to be $E_{V-I} \simeq 0.16$ mag. Moreover, it is very close to HD 64503, a bright star with $V \sim 4.5$. This explains some of the stray light seen over the images available for this field. Nevertheless, both the galactocentric distance and distance from the plane (MacMinn et al. 1994) make Berkeley 20 the most distant known open cluster, and a better determination of its metallicity and age would help trace the formation and evolution of the galactic disk.

Due to the cluster distance, the field covered by WFI leads to a high foreground contamination. In order to minimize this effect the CMD shown in Fig. 9 includes only objects within a circular region with 3 arcmin radius around the nominal center of this open cluster. Within this region, the CMD shows a well-defined turnoff at $V \simeq 18.25$ and $B-V \simeq 0.6$. There are also a number of blue-straggler candidates. However, no red clump is visible in the CMD shown in Fig. 9. On the other hand, if one inspects the CMD obtained using a larger radius ($\sim$10 arcmin) a small and isolated number of stars are found around $V \simeq 16.30$ and $(B-V) \simeq 1.1$. While at such distance from the cluster center it is difficult to discriminate cluster members from field stars, it is interesting to note that the location of this concentration would coincide with the red clump of M 67 (applying the appropriate scaling for the cluster distance). This result is consistent with the conclusions of MacMinn et al. that the general features of Berkeley 20 CMD are similar to those of M 67, even though no red clump was identified in their data. This shows the great value of the wide-area coverage of the PF data. Follow-up observations with FLAMES could settle this question.

7.2.3. NGC 2477

In contrast to the previous systems, NGC 2477 is a relatively young cluster ($1^{+0.3}_{-0.2}$ Gyr) located at a distance of $(m-M)_0 = 10.61$ (Kassis et al. 1997). Unfortunately, as shown by Kassis et al. and Majewski et al. (2000), NGC 2477 suffers from differential reddening, and both groups adopted a reddening range $E_{B-V} = 0.2 - 0.4$ determined by Hartwick et al. (1972). Friel & Janes (1993) determined a metal abundance of [Fe/H]$= -0.5 \pm 0.11$ using moderate resolution spectroscopy of seven cluster giants.

The CMD of NGC 2477 shows that the MS of the cluster is well-defined from $V \simeq 12.7$ to $V \simeq 22$. The TO of the cluster is located around $(B-V) \simeq 0.50$, at about the same magnitude of the red clump ($V \simeq 12.75$) seen at $(B-V) \sim 1.2$. The effect of the differential reddening is evident at the TO magnitude, which widens the MS near the TO. Finally, some blue-stragglers candidates are found at $(B-V) \simeq 0.2$ and $V \lesssim 12$.

A population of blue objects ($(B-V) \lesssim 0.6$) is present at $V \gtrsim 18$. However, the density of points in this region is far less than that seen in the CMD presented by Kassis et al. (1997) over a smaller area (15×15 square arcmin). A smaller density is also found by Majewski et al. (2000), even though in a different magnitude system. Furthermore, the blue population of Kassis et al. is spread over a large range of colors and does not seem to define any clear sequence which could reflect the WD cooling sequence. While the blue population observed with the present data may be associated with white dwarfs, as hinted by the presence of few faint stars around $V \sim 20$ and $(B-V) \simeq 0.2$, the Kassis et al. seem to considerably overestimate the density of these objects. The reasons for that are at the present time not clear.

One prominent feature of the NGC 2477 CMD is the substantial contribution of background field stars, which is independent of the region around the cluster considered. Fortunately, the contamination is concentrated in a well-defined color range ($0.8 < (B-V) < 1.6$) at magnitudes $V \gtrsim 18.0$, not severely affecting the MS of the cluster, except where it intersects the cluster MS around $V \sim 18$. The effect of the contamination, by field giant stars, is also seen at brighter magnitudes and redder colors, almost overlapping the cluster's red clump.

7.2.4. NGC 2506

This cluster has been studied by McClure et al. (1981) over a 10 arcmin diameter field of view, using photoelectric photometry, and by Marconi et al. (1997), who obtained CCD photometry of an area of 6×6 arcmin. The present data reach almost four magnitudes deeper than any previous study of this system, covering at the same time a much larger area, at least 10 times the size. NGC 2506 is a relatively old open cluster but its exact age is very uncertain, varying from 1.5–3.4 Gyr. Marconi et al. estimate 1.5–1.7 Gyr, in reasonable agreement with the value of 1.9 Gyr found by Carraro & Chiosi (1994), while McClure et al. (1981) estimate an age of 3.4 Gyr.

For this cluster Fig. 10 shows only objects within a circular region 5 arcmin in radius. The CMD of this region shows a well-defined MS closely resembling that presented by Marconi et al. In this case, differential reddening may be important. Schlegel et al. (1998) estimate $E_{B-V} = 0.087$ mag. Contamination of the MS by field stars is seen primarily as a vertical sequence around $(B-V) \simeq 0.6$. However, the group of stars bluer than $(B-V) \simeq 0.4$ and fainter than $V \sim 21$ can conceivably be the tip of the white dwarf cooling sequence associated with the cluster. These stars are particularly interesting for follow-up observations with FLAMES. At magnitudes brighter than the TO ($V = 14.7$), a small number of blue-straggler candidates are also seen. More candidates can be found if one considers a larger area than the one shown in Fig. 10.

Several issues related to this cluster could be addressed with FLAMES. In particular, a better and direct determination of its metallicity. Friel & Janes (1993) measured [Fe/H]$= -0.52 \pm 0.07$ from medium-resolution spectroscopy of five cluster members, while Marconi et al. using different stellar evolutionary models can fit the observed data either with values of metallicity consistent with that determined spectroscopically or with solar values.

7.2.5. Small Magellanic Cloud fields

The Magellanic Clouds are ideal targets for the study of galaxy formation and evolution. Their proximity has enabled ground-based observations to unveil their oldest populations and resolve them into individual stars. Moreover, both the LMC and SMC contain young, rich cluster systems that span a wide range of ages and metallicities, evidence of their extended star formation history. The young clusters offer a unique opportunity to study the properties of massive stars and to compare them with predictions of stellar evolutionary models. Such studies might provide insight into the physical processes responsible for their evolution, such as the treatment of mixing.

This PF release includes two adjacent fields in the SMC. The combined V image produced by the stacking of the two DEEP exposures of one of the SMC fields (SMC 5) is shown in Fig. 1. The image shows a uniformly distributed population of SMC "field stars", presumably the old population, and a considerable number of young star clusters. In SMC 5 the following clusters can be identified: NGC 346, NGC 330, IC 1611, NGC 306, NGC 299, OGLE 109, OGLE 119, OGLE 99. From an inspection of a similar image for SMC 6 one finds the clusters: OGLE 124, IC 1624, OGLE 129, K 50, OGLE 134, K 54. These images show the great contribution of a wide-field imager to the study of such nearby systems. The two fields of SMC being released provide a large survey of OB associations which can be immediately observed with FLAMES. One of the fields (SMC 5) includes the brightest HII region (NGC 346) of the SMC. Massey et al. (1989) confirm the presence of 33 O stars, 11 of which are of type O6.5 or earlier. Six stars were found in the mass range 40−80 $M_{\odot}$. They also identified few red supergiants of considerably lower mass (15 $M_{\odot}$) concentrated in a spatially distinct subgroup. From a close inspection of the image shown Fig. 1 the existence of this distinct subgroup is confirmed at $\alpha = 00^{\rm h}59^{\rm m}05.2^{\rm s}$ and $\delta = -72^{\circ}09^{\rm m}15.4^{\rm s}$.

The CMD of the two SMC fields show a number of populations with different ages and metallicities, ideal targets for FLAMES. Note that the CMD of SMC 5 reaches fainter magnitudes compared to that of SMC 6. This is because only one DEEP V image is available for SMC 6. The most prominent feature of both SMC CMDs is the MS centered around $(B-V) \simeq -0.2$, as expected from the low reddening towards the SMC ($E_{B-V} = 0.037$, Schlegel et al. 1998). The broadening of the MS at faint magnitudes ($V \lesssim 20$) can be due to several effects such as crowding and increasing photometric errors. For magnitudes $V \lesssim 17$ the broadening is mainly caused by blue supergiants. The MS terminates around $V \simeq 14.3$ while the blue supergiants extend up to $V \simeq 12.5$. At redder colors ($0.5 \lesssim (B-V) \lesssim 2.0$) there is another tilted sequence which corresponds to the red end of the blue loop (red supergiants). In between the blue and red-end of this loop, there is an almost vertical sequence starting at $V \simeq 19.5$, $(B-V) \simeq 0.7$, which extends at least to $V \simeq 13.5$. This population is the so-called "vertical clump" (Gallart et al. 1998) formed by young (few hundred Myr to 1 Gyr old), core He-burning and intermediate-mass stars. Note, however, that this sequence might suffer contamination by foreground stars and supergiants along the loop. At $(B-V) \sim 1.6$ and $V \sim 17$ one sees the tip of a broad red giant branch (RGB). The width of the RGB at the tip is ∼0.45 mag. This is probably due to the combined effects of age and metallicity. Finally, even though hard to identify, given the resolution of the Fig. 10, the red extension of the horizontal branch is visible at $V \sim 19.5$ in the color interval $0.4 \lesssim (B-V) \lesssim 0.6$. However, one finds no evidence of a blue horizontal branch.

The CMD shown in Fig. 10 reflects primarily the properties of the SMC field star population. However, as mentioned above the two SMC fields observed so far contain at least 14 stellar systems, whose CMDs can also be extracted from the same data. Despite possible contamination problems, such analysis is of great interest to study the star formation history of both cluster and field populations.

7.3. Future work

As discussed above, the data presented here provides not only the means for producing target lists for FLAMES but also a wealth of information about a variety of stellar systems. Furthermore, the data from the survey can be combined to other data sets which can greatly enhance the scientific value of the survey.

As an example, for all the observed fields the final color catalogs were associated with those being produced by the 2MASS survey. Combined EIS and 2MASS data will provide a six passband multi-color data sets. As an illustration the upper panel of Fig. 11 shows the optical/infrared $V, (B-K)$ CMD obtained for M 67. Among many interesting features, it is worth noticing how the MS of M 67 (Fig. 9) is resolved into two well-defined parallel sequences, much more clearly than using the optical alone. The binary sequence is clearly visible in the magnitude interval $14.5 \lesssim V \lesssim 18$. Moreover, and in addition to the well-known gap at $V \sim 13$, the diagram shows clear evidence of another gap at $V \sim 16.15$ and $(B-K) \sim 3.35$. The lower panel of Fig. 11 shows the $K, (B-K)$ CMD for SMC 5. In contrast to the optical CMD, the optical/infrared provides a clear view of the lower temperature stars, while the hot MS and blue supergiants essentially disappear. In this diagram both the red supergiant and the red giant

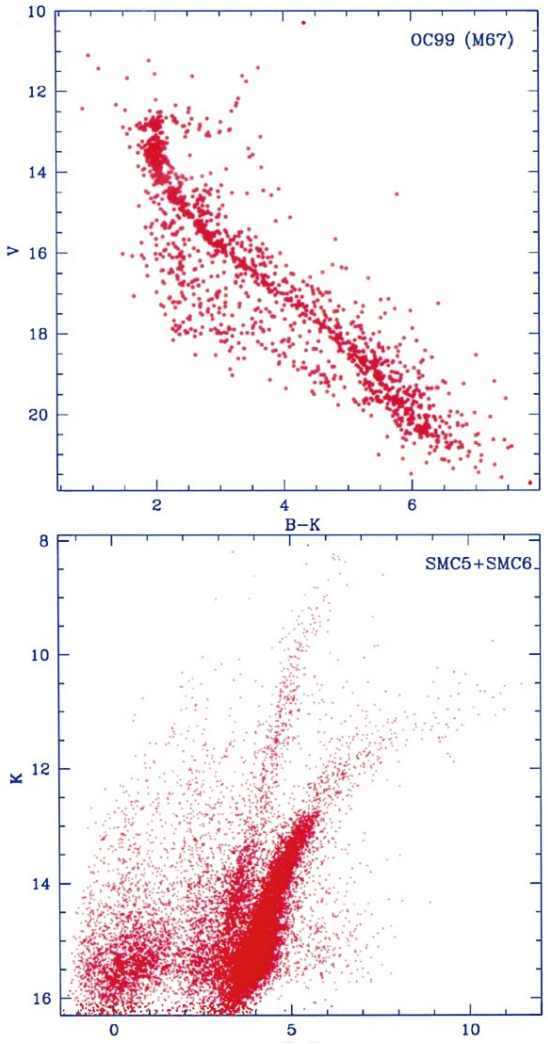

Fig. 11. The optical/infrared color-magnitude diagram obtained for M 67 combining EIS and 2MASS data.

sequences are clearly visible and more easily distinguishable. Also note the asymptotic giant branch (AGB) stars ($K \lesssim 12.5$) starting from $(B-K) \gtrsim 5.5$ and extending to extremely red colors ($(B-K) \sim 11.2$). Stars found in this region resemble those found by Nikolaev & Weinberg (2000), studying the 2MASS diagram of the LMC, and interpreted as Carbon-rich Thermally-Pulsating AGB and long period variables. In the blue part of the diagram some MS and blue supergiants are still present, and seem to be separated. In addition, there is a hint of a population along the blue loop ($K \sim 15.5$ and $0.5 < (B-K) < 2.5$). Thus, the color baseline provided by the combination of optical and infrared data, is a powerful tool in separating the different populations of composite systems.

Lastly, combining the optical and infrared data may also allow for the spectral classification of objects by matching the photometric measurements against template spectra (Hatziminaoglou et al. 2001). This may help further disentangle different populations and search for particular types of stars. Results from such an analysis will be presented in a subsequent paper of this series.

8. Summary

This paper presents the first set of fully-calibrated images and catalogs of the PF survey. The data presented here have been used to evaluate the observing strategy, data reduction, catalog production and preparation of target lists for feeding the FLAMES fiber positioner. Particular emphasis has been given to the accuracy of the astrometric calibration. The analysis presented in this paper has shown the need for some improvement in the software, currently underway, in order to efficiently cope with the large amount of data already available. From a comparison of the results obtained using different reference catalogs, one finds that while the USNO 2.0 provides adequate astrometric solutions, with accuracy within the requirements of FLAMES, future reductions should be done with the recently released GSC 2.2 catalog. The latter proved to be far superior with less systematics and smaller uncertainties.

The color catalogs produced have been used to derive color-magnitude diagrams for all the fields considered. The CMDs span 13 mag in V which ensures a better selection of both bright and faint targets for FLAMES. A comparison of the CMDs with those of other authors show good agreement over the magnitude range in common. However, the PF data are far superior given their extended magnitude and area coverage. Furthermore, combining these data with ongoing surveys in other wavelengths gives additional leverage for the identification of different stellar populations, of key importance for the envisioned FLAMES programs.

All the specific software developed to deal with the PF survey data is currently being incorporated into the EIS survey system framework. This should allow the efficient reduction of all of the remaining data gathered by this survey. The fully calibrated images and catalogs presented in this paper will be used in the commissioning phase of FLAMES and can be requested from the URL "`http://www.eso.org/eis`".

Acknowledgements. We thank L. Pasquini for having promoted the Pre-FLAMES survey and for his constant encouragement. We also thank A. Renzini for his continuing support of the EIS project. F. Comeron, V. Hill, and F. Primas are thanked for their support in the preparation of the original proposal. We would also like to acknowledge F. Ferraro, V. Hill, J. Krautter, J. Mermillod, B. Nordström, S. Ortolani, G. Piotto, F. Primas, S. Randich and E. Tolstoy for their suggestions in the initial phase of selection of the Pre-FLAMES targets. Y.M. thanks the Università di Padova, E. V. Held, G. Piotto & S. Ortolani. S.Z., thanks the Osservatorio di Trieste. We also thank M. Zoccali for careful reading of the paper, and L. Rizzi for useful discussions on WFI calibration. The Guide Star Catalogue-II is produced by the Space Telescope Science Institute in collaboration with the Osservatorio Astronomico di Torino. Space Telescope Science Institute is operated by the Association of the Universities for Research in Astronomy, for the National Aeronautics and Space Administration under contract NAS5-26555. Additional support is provided by the Association of Universities for Research in Astronomy, the

Italian Council for Research in Astronomy, European Southern Observatory, Space Telescope European Coordinating Facility, the International GEMINI project and the European Space Agency Astrophysics Division. This publication makes use of data products from the Two Micron All Sky Survey, which is a joint project of the University of Massachusetts and the Infrared Processing and Analysis Center/California Institute of Technology, funded by the National Aeronautics and Space Administration and the National Science Foundation. This research has made use of the SIMBAD database, operated at CDS, Strasbourg, France.

References

Arnouts, S., Vandame, B., Benoist, C., et al. 2001, A&A, 379, 740
Carraro, G., & Chiosi, C. 1994, A&A, 288, 751
Dinescu, D. I., Demarque, P., Guenther, D. B., & Pinsonneault, M. H. 1995, AJ, 109, 2090
Friel, E. D., & Janes, K. A. 1993, A&AS, 267, 75
Gallart, C. 1998, ApJL, 495, L43
Girard, T. M., Grundy, W. M., Lopez, C. E., & van Altena, W. F. 1989, AJ, 98, 227
Hartwick, F. D. A., Hesser, J. E., & McClure, R. D. 1972, ApJ, 174, 557
Hatziminaoglou, E., et al. 2001, A&A, submitted
Kassis, M., Janes, K. A., Friel, E. D., & Phelps, R. L. 1997, AJ, 113, 1723
Landolt, A. U. 1992, AJ, 104, 340
MacMinn, D., Phelps, R. L., Janes, K. A., & Friel, E. D. 1994, AJ, 107, 1806
Majewski, S. R., Ostheimer, J. C., Kunkel, W. E., & Patterson, R. J. 2000, AJ, 120, 2550
Marconi, G., Hamilton, D., Tosi, M., & Bragaglia, A. 1997, MNRAS, 291, 763
Massey, P., Parker, J. W., & Garmany, C. D. 1989, AJ, 98, 1305
Mathieu, R. D. 1985, in Proc. IAU Symp. 113, Dynamics of Star Clusters, ed. J. Goodman, & P. Hut (Dordrecht: Reidel), 427
McClure, R. D., Twarog, B. A., & Forrester, W. T. 1981, ApJ, 243, 841
McLean, B., Greene, G., Lattanzi, M., & Pirenne, B. 2000, Astronomical Data Analysis Software and Systems IX, ed. N. Manset, C. Veillet, & D. Crabtree, ASP Conf. Proc., 216, 145
Montgomery, K. A., Marschall, L. A., & Janes, K. A. 1993, AJ, 106, 181
Nikolaev, S., & Weinberg, M. D. 2000, ApJ, 542, 804
Pasquini, L., & Belloni, T. 1998, A&A, 336, 902
Pasquini, L., et al. 2000, SPIE, 4008, 129
Phelps, R. L., Janes, K. A., & Montgomery, K. A. 1994, AJ, 107, 1079
Renzini, A., & da Costa, L. N. 1997, The Messenger, 87, 23
Richer, H. B., Fahlman, G. G., Rosvick, J., & Ibata, R. 1998, ApJL, 504, L91
Schlegel, D. J., Finkbeiner, D. P., & Davis, M. 1998, ApJ, 500, 525
Stetson, P. B. 1987, PASP, 99, 191
Tautvaisiene, G., Edvardsson, B., Tuominen, I., & Ilyin, I. 2000, A&A, 360, 499
Vallenari, A., Ortolani, S., & Chiosi, C. 1994, A&AS, 108, 571
Vandame, B., Olsen, L. F., Jorgensen, H. E., et al. 2001, A&A, submitted